Proceedings of the
International Conference on Mechanical Engineering 2011
(ICME2011) 18-20 December 2011, Dhaka, Bangladesh

ICME11-FL-018

APPLICATION OF DYNAMIC NONLINEAR SUBGRID-SCALE STRESS MODEL FOR THE PULSATILE FLOW IN A BOTH SIDED CONSTRICTED CHANNEL

Afzal Hossain[1], **Md. Mamun Molla**[2] **and Bing-Chen Wang**[1]

[1]Dept. of Mechanical and Manufacturing Engg., Univ. of Manitoba, Canada.
[2]Dept. of Electrical and Computer Science, North South University, Dhaka, Bangladesh.

ABSTRACT

The technique of large-eddy simulation (LES) is applied for the laminar transition-to-turbulent physiological pulsatile flow in a 3D model of stenosis. LES has been applied to numerical investigation of transition-to-turbulent pulsatile flows [1, 2] with the conventional dynamic subgrid-scale (SGS) stress model (DM) of Lilly [3] in which the Smagorinsky constant is not allowed to be negative values due to the potential numerical instability. Here we implement the advanced dynamic nonlinear SGS modelling (DNM) of Wang and Bergstrom [4] which is proved to be more robust than the conventional DM if the model coefficients are allowed to be negative. Results from the simulations show that the DNM is flexible in self-calibration of its model coefficients with local stability in the context of a physiological pulsatile laminar-turbulent transitional flow. A variety of statistics have been presented in terms of the resolved mean velocity, wall shear stress, resolved and subgrid-scale Reynolds stresses etc. along with the grid sensitivity test using three different grid arrangements.

Keywords: Large-Eddy Simulation, Model Stenosis, Dynamic Nonlinear Subgrid-Stress Model.

1. INTRODUCTION

Investigation of fluid flow through stenosed (constricted) geometry has become quite interesting for its significance in biomechanics from theoretical, experimental and clinical point of view. Generally the blood flow through arteries is unsteady and pulsatile due to the cyclic nature of heart pump. The Reynolds number of blood flow can vary from 1 to 4000 in different types of arteries [5]. Though blood flow is usually pulsatile laminar without any obstruction in the artery, it undergoes a phase of transitional-to-turbulent in presence of a constriction. On the other hand, flow pulsatility also plays an important role on transition to turbulence in arteries [5]. As a result, due to the presence of stenosis and flow pulsatility, turbulence can generate even at a Reynolds number as low as a few hundred [6].

Numerous experimental studies have been performed for getting a better insight of the transition-to-turbulent flow through arterial stenosis. Most of the experimental studies of blood flow through stenosis model have focused on the poststenotic flow physics and the effects of blood vessel geometries and shear stresses on the inner arterial wall. Clark *et al.* [7, 8] performed steady and pulsatile flow experiments with a nozzle type laboratory model of arterial stenosis and demonstrated the different regions of flow produced by stenosis. Measurement of velocity energy spectra for a variety of stenosis shapes and flow conditions and effect of Reynolds number on the disturbance of velocity was also reported by him. Characteristics of the flow disorder over a transitional Reynolds number range as well as the relationship of steady to pulsatile flow through mild and moderate degrees of occlusion is studied by Cassanova and Giddens [9]. They conducted experiments through modeled stenosis for Reynolds number ranging from 318-2540 (based on the tube diameter and mean velocity) and a pulsatile frequency parameter of 15. Ahmed and Giddens [10, 11] also studied the velocity and flow disturbance measurements through axisymmetric stenosis of 25%, 50% and 75% area reduction at the moderate Reynolds number in the range from 500 to 2000 using Laser Doppler Anemometry. Their results indicate that the flow disturbances of discrete oscillation frequency are the most important indicator of early stage of stenosis development.

Beyond these leading experimental investigations mentioned above, the method of computational fluid dynamics (CFD) has been significantly developed to simulate this type of flow over the past decade. Several CFD studies have been reported on laminar-turbulent transition flow in idealized stenoses with different turbulent methodologies: Reynolds-averaged Navier-

Stokes (RANS), direct numerical simulation (DNS) and large-eddy simulation (LES). From the point of view of computational modeling, DNS is extremely taxing on computing resources as all the spatial and temporal scales of turbulence are accurately solved. On the other hand, RANS turbulence models are primarily designed for simulating well-developed, high Reynolds number turbulent flows and are not suitable for arterial flows. Owing to the limitations of the RANS and DNS approaches mentioned above, the method of LES, where a filter is used to differentiate large (filtered) and small (subgrid) scales of motion, embodies a superior numerical tool for this type of research. The application of the technique of LES to the study of flow in a modeled arterial stenosis was presented by Mittal *et al*. [12]. Molla *et al*. [2, 13] also investigated with the same type of model stenosis for both additive and non-additive pulsatile flow for a maximum Reynolds number 2000 using the dynamic model (DM) of Lilly [3] and reported the turbulent phenomena at the post-stenotic region with the pulsation effects. It is observed from the literature survey that, most of the LES studies are based on the conventional dynamic subgrid-scale (SGS) stress model (DM) of Lilly [3] as well as Boussinesq eddy viscosity approximation. One of the important drawbacks of this model is linked to the overly simplistic constitutive relation adopted in the model. On one hand, if the model coefficient is restricted to be positive, it can lead to an unrealistic SGS dissipation effect. On the other hand, if the coefficient is allowed to be negative, numerical instability arises due to excessive backscatter of the SGS turbulent kinetic energy (TKE). Here we implemented the advanced dynamic nonlinear SGS modeling (DNM) of Wang and Bergstrom [4] which includes the conventional DM as its first-order approximation as well as two higher-order tensorial constituent components for nonlinear anisotropic representation of the SGS stress tensor.

In this paper, we numerically investigate pulsatile laminar-turbulent transitional flow in a 3D channel with a biological type stenosis formed axi-symmetrically on the top and bottom walls based on the advanced dynamic nonlinear SGS model.

2. FORMULATION OF THE PROBLEM

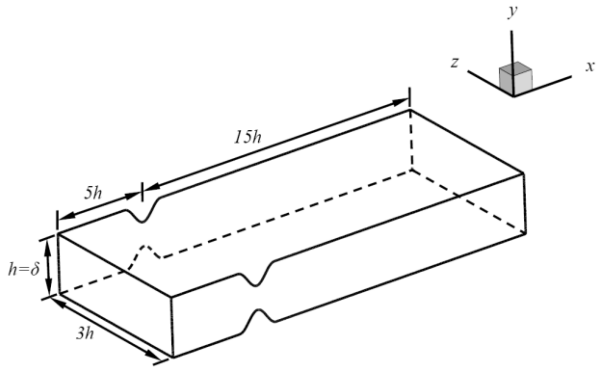

Fig 1. Schematic of an idealized stenosis model and the associated coordinate system

The geometry shown in Fig 1. consists of a 3D channel with a both sided cosine shaped stenosis on the upper and lower wall centred at *x/h* =0.0, where *x* is the horizontal distance or the distance along the flow and *h* is the height of the channel. In the figure, we use *x*, *y* and *z* to represent the streamwise, vertical and spanwise coordinates, respectively. The stenosis is centered 5*h* downstream of the channel inlet and 15*h* away from the channel outlet. The stenosis is formed using the following geometrical relationship:

$$\frac{y}{h} = 1 - \delta_c \left(1 + \cos\frac{x\pi}{h}\right), \qquad -\frac{h}{2} \le x \le \frac{h}{2}$$

where δ_c is the parameter that relates to the area reduction of the stenosis. δ_c is fixed to 0.5 , which gives a 50% reduction of the cross-sectional area from top and bottom wall at the centre of the stenosis.

2.1 Governing Equations

The blood flow in a large vessel can be modeled accurately as a Newtonian fluid and it allows us to use the Navier-Stokes equations of motion for investigating post-stenotic flow through arterial stenosis. The equations of motion for variables that have been spatially filtered on the scale of their spatial resolution is given by,

$$\frac{\partial \bar{u}_i}{\partial x_i} = 0 \tag{1}$$

$$\frac{\partial \bar{u}_i}{\partial t} + \frac{\partial}{\partial x_j}(\bar{u}_i \bar{u}_j) = -\frac{1}{\rho}\frac{\partial \bar{P}}{\partial x_i} + \upsilon \frac{\partial^2 \bar{u}_i}{\partial x_j \partial x_j} - \frac{\partial \tau_{ij}}{\partial x_j} \tag{2}$$

2.2 Dynamic Nonlinear SGS Stress Model (DNM)

The DNM of Wang and Bergstrom [4] is used to evaluate the SGS stress tensor τ_{ij} appearing in the filtered momentum Eq. (2). The constitutive relation for the DNM is based on the explicit nonlinear quadratic tensorial polynomial constitutive relation.

$$\tau_{ij}^* = -C_S \beta_{ij} - C_W \gamma_{ij} - C_N \eta_{ij} \tag{3}$$

where an asterisk represents a trace-free tensor, i.e. $(\cdot)_{ij}^* \triangleq (\cdot)_{ij} - (\cdot)_{kk}\,\delta_{ij}/3$, and the base tensors are defined as $\beta_{ij} \triangleq 2\bar{\Delta}^2|\bar{S}|\bar{S}_{ij}$, $\gamma_{ij} \triangleq 4\bar{\Delta}^2(\bar{S}_{ij}\bar{\Omega}_{ij} + \bar{S}_{jk}\bar{\Omega}_{ki})$ and $\eta_{ij} \triangleq 4\bar{\Delta}^2(\bar{S}_{ik}\bar{S}_{kj} - \bar{S}_{mn}\bar{S}_{nm}\,\delta_{ij}/3)$. Here, $\bar{\Delta} \triangleq (\Delta x \Delta y \Delta z)^{1/3}$ is the grid-level filter width; δ_{ij} is the Kronecker delta; $\bar{S}_{ij} \triangleq \frac{1}{2}(\frac{\partial \bar{u}_i}{\partial x_j} + \frac{\partial \bar{u}_j}{\partial x_i})$ and $\bar{\Omega}_{ij} \triangleq \frac{1}{2}(\frac{\partial \bar{u}_i}{\partial x_j} - \frac{\partial \bar{u}_j}{\partial x_i})$ are the resolved strain and rotation rate tensors, respectively; and $|\bar{S}| = (2\bar{S}_{ij}.\bar{S}_{ij})^{1/2}$. According to Wang and Bergstrom [4], the values of the three model coefficients C_S, C_W and C_N can be determined by minimizing the residual of the Germano identity following the dynamic procedure of Lilly [3] as

$$\begin{bmatrix} M_{ij}M_{ij} & M_{ij}W_{ij} & M_{ij}N_{ij} \\ W_{ij}M_{ij} & W_{ij}W_{ij} & W_{ij}N_{ij} \\ N_{ij}M_{ij} & N_{ij}W_{ij} & N_{ij}N_{ij} \end{bmatrix} . \begin{bmatrix} C_S \\ C_W \\ C_N \end{bmatrix} = - \begin{bmatrix} L_{ij}^* M_{ij} \\ L_{ij}^* W_{ij} \\ L_{ij}^* N_{ij} \end{bmatrix} \tag{4}$$

where $L_{ij} \triangleq \widetilde{\bar{u}_i \bar{u}_j} - \tilde{\bar{u}}_i \tilde{\bar{u}}_j$ is the resolved Leonard type stress; $M_{ij} \triangleq \alpha_{ij} - \tilde{\beta}_{ij}$, $W_{ij} \triangleq \lambda_{ij} - \tilde{\gamma}_{ij}$ and $N_{ij} \triangleq \zeta_{ij} - \tilde{\gamma}_{ij}$ are differential tensors respectively; and $\alpha_{ij} \triangleq 2\tilde{\bar{\Delta}}^2|\tilde{\bar{S}}|\tilde{\bar{S}}_{ij}$, $\lambda_{ij} \triangleq 4\tilde{\bar{\Delta}}^2(\tilde{\bar{S}}_{ik}\tilde{\bar{\Omega}}_{kj} + \tilde{\bar{S}}_{jk}\tilde{\bar{\Omega}}_{ki})$ and

$\zeta_{ij} \triangleq 4\widetilde{\bar{\Delta}}^2(\tilde{\bar{S}}_{ik}\tilde{\bar{S}}_{kj} + \tilde{\bar{S}}_{mn}\tilde{\bar{S}}_{nm}\,\delta_{ij}/3)$ are base tensors at the test-grid level.

2.2 Boundary Conditions

The physiological pulsatile laminar velocity profile, which is used to generate the time dependent pulsatile flows at the inlet of the channel, is obtained through an analytical solution to the Navier-Stokes equation in the context of a fully-developed laminar channel flow. The solution is as follows:

$$\bar{u}(y,t) = 4\bar{U}\left(\frac{1}{4} - \frac{y^2}{h^2}\right) + A\sum_{n=1}^{N}\frac{h^2}{in\mu\alpha^2}\left[1 - \frac{\cosh\left(\sqrt{in}\,\alpha\frac{y}{h}\right)}{\cosh\left(\sqrt{in}\,\alpha\frac{1}{2}\right)}\right]e^{i(n\omega t + \phi_n)} \quad (5)$$

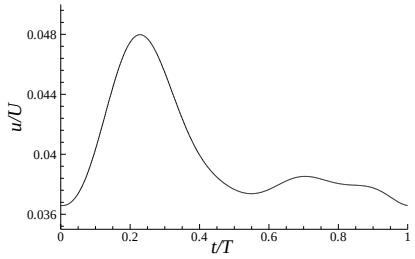

Fig 2. Temporal variation of inlet velocity profile, $\bar{u}/\bar{U}$ near the wall

Fig 2. shows the temporal variation of the inlet velocity profile derived from the Eq. (5) for *Re* = 2000. The pulsatile laminar velocity profile is used to generate the time-dependent pulsatile flows at the inlet of the channel. No-slip and impermeable boundary conditions are applied to all solid surfaces. The zero-gradient boundary condition is employed at the outlet of the channel, and periodical boundary conditions are applied in the spanwise direction.

3. NUMERICAL PROCEDURE

A finite volume method is used to discretise the governing filtered equations to yield a system of linear algebraic equations. To discretise the diffusion term, a second-order accurate central difference scheme is used. For the convective term, an energy conserving discretisation scheme is used. The transient term is discretised using a three point backward difference scheme with a constant time step Δt=1.5×10−3 seconds. A pressure correction algorithm is applied to the coupled pressure with the velocity components stored at the centre of a control volume in accordance with the collocated grid arrangement. At each time step, the pressure field was updated by solving a Poisson type pressure correction equation using an ICCG [14] method. The checkerboard effect in the pressure field arising from the pressure-velocity decoupling on a collocated grid system was removed using a nonlinear momentum interpolation scheme. A BI-CGSTAB [15] solver is used for solving the matrix of velocity vectors. Overall the code is second-order accurate in both time and space.

4. RESULTS ANALYSIS

Two Reynolds number (i.e. 1000 and 2000) are considered for the present study with a grid sensitivity test for three different grid systems, 50×150×40 (Case 1), 70×180×40 (Case 2) and 50×210×40 (Case 3) control volumes (in the stream, vertical and spanwise directions, respectively). In order to resolve the wall shear stress in the near wall region, the grid is refined significantly in the spanwise direction. Fig 3 and Fig 4 depict the results for three cases are compared in terms of non-deimensionalized time-averaged streamwise velocity ($<\bar{u}>/\bar{U}$) and resolved TKE ($k/\bar{U}^2$) respectively, at different location along the streamwise direction. It is obvious from Fig 3 that these above

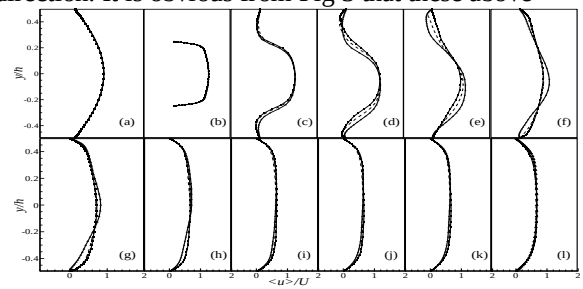

Fig 3. Grid sensitivity test with respect to the mean streamwise velocity, $<\bar{u}>/\bar{U}$, at (a) *x/h* = -5, (b) *x/h* = 0, (c) *x/h* = 1, (d) *x/h* = 2, (e) *x/h* = 3, (f) *x/h* = 4, (g) *x/h* = 5, (h) *x/h* = 6, (i) *x/h* = 8, (j) *x/h* = 10, (k) *x/h* = 12, (l) *x/h* = 15. Based on three grid systems, Case 1: solid line for $50 \times 150 \times 40$ control volumes, Case 2: dashed line for $70 \times 180 \times 40$ control volumes, Case 3: solid line with symbol for $50 \times 210 \times 40$ control volumes.

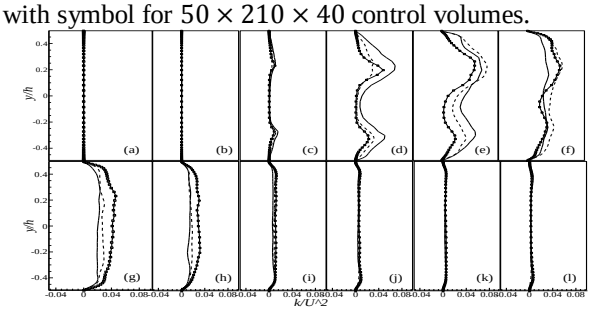

Fig 4. Grid sensitivity test with respect to the TKE, $k/\bar{U}^2$, at (a) *x/h* = -5, (b) *x/h* = 0, (c) *x/h* = 1, (d) *x/h* = 2, (e) *x/h* = 3, (f) *x/h* = 4, (g) *x/h* = 5, (h) *x/h* = 6, (i) *x/h* = 8, (j) *x/h* = 10, (k) *x/h* = 12, (l) *x/h* = 15. Based on three grid systems, Case 1: solid line for $50 \times 150 \times 40$ control volumes, Case 2: dashed line for $70 \times 180 \times 40$ control volumes, Case 3: solid line with symbol for $50 \times 210 \times 40$ control volumes.

mentioned cases are sufficient to resolve the mean velocity fields, though Fig. 6 shows a slight variation of non-dimensionalized TKE at the immediate post-stenotic region 1< *x/h* <6. The 70×180×40 grid arrangement (Case 2) is selected for presenting the results in the remainder part of the paper.

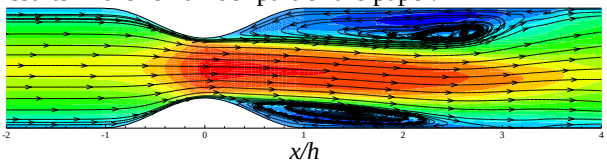

Fig 5. Time mean streamlines appended on the streamwise mean velocity, $<\bar{u}>/\bar{U}$ for *Re* = 2000.

Fig 5. illustrates the time-averaged streamlines at the central plane (z/h=0.5) for Re=2000. Two recirculation regions, one in the lower wall and another in the upper wall are observed near the post lip of the stenosis due to the separation of the shear layer from the nose of the stenosis. The recirculation region in the upper wall is larger than that in the lower wall. These recirculation regions are responsible for critical medical conditions. At Re = 2000, the location of separation of the recirculation zones is $x/h|s$ = 0.107, and the location of reattachment is $x/h|r$ = 2.15, respectively.

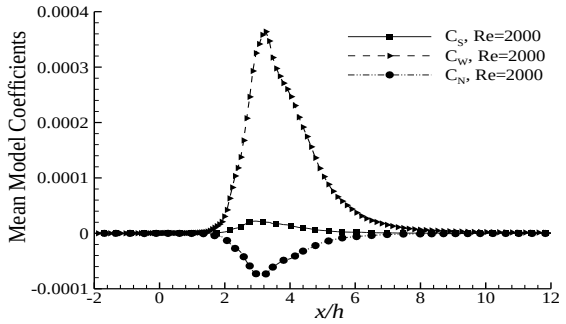

Fig 5. Time and spanwise averaged DNM coefficients, $<C_S>$, $<C_W>$ and $<C_N>$ at y/h = 0.5 for Re = 2000.

Fig 5. shows the streamwise distribution of time and spanwise averaged DNM coefficients. From the figure, we can see that all the three DNM coefficients approaches to zero in the regions x/h<1.8 and x/h>8.3. It implies that the flow pattern is laminar due to the dominant viscous forces in those regions. In the core region of turbulence, the mean value is positive for $<C_S>$ and $<C_W>$ but negative for $<C_N>$. Moreover, the DNM coefficients reach their maximum values in the region 2.5<x/h<3.3.

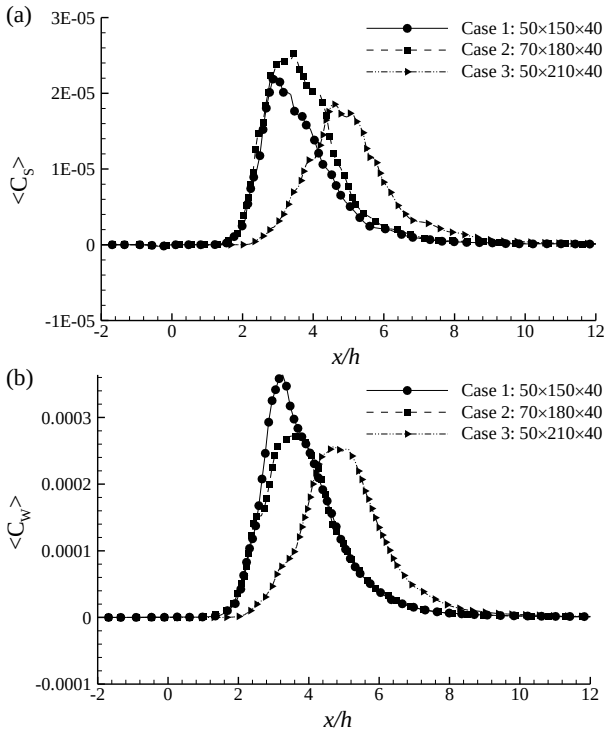

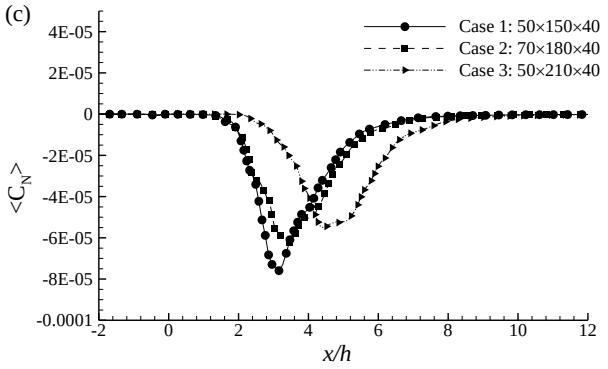

Fig 6. Sensitivity of the time and spanwise averaged DNM coefficients to grid resolution for Re = 2000 at y/h = 0.5.

Fig 6. compares the model coefficients calculated for Re = 2000 using the three different grid arrangements. The values obtained using the three grid arrangements are slightly different to account for the grid effects. From these three figures we may conclude that the magnitude of $<C_W>$ is one order higher than the $<C_S>$ with same sign, but the order of $<C_N>$ is same with the opposite sign.

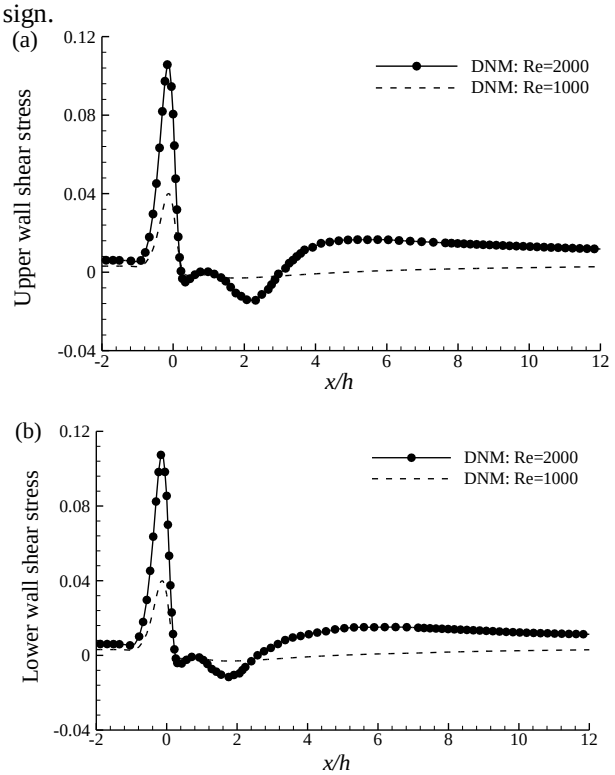

Fig 7. Non-dimensionalized time-averaged wall shear stress,$< \tau_w > / \rho \bar{U}^2$, at (a) upper wall and (b) lower wall.

Time-averaged wall shear stress, $< \tau_w > / \rho \bar{U}^2$ at both the upper and lower walls for Re =1000 and 2000 are presented in Fig. 7(a) and 7(b). Both at the upper and lower walls there is an acute shear stress rise just prior to the centre of the stenosis. This occurs due to the acute pressure drop across the stenosis. It is also observed that the magnitude of the maximum wall stress increases with the Reynolds number.

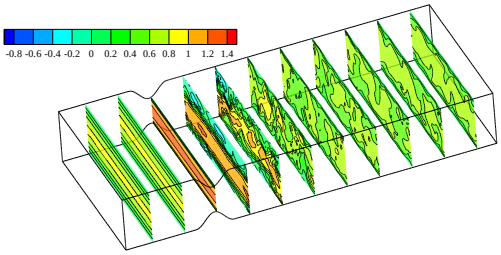

Fig 8. Slice view of instantaneous streamwise velocity, $< \bar{u} > / \bar{U}$ for *Re* = 2000 at *t/T* = 10.25.

The slice view of the isopleths of the instantaneous stremwise velocity, $< \bar{u} > / \bar{U}$, is shown in Fig. 8 at *t/T* = 10.25 for *Re* = 2000. The first two slices show that prior to the stenosis, the flow is laminar and stratified. The third slice shows that the velocity reaches maximum (due to continuity) at the throat of the stenosis. The large velocity in the fourth and fifth slices (indicated by reddish color) reflects the immediate post-stenotic region. The following slices represent that the flow is becoming re-laminarized gradually in the downstream region.

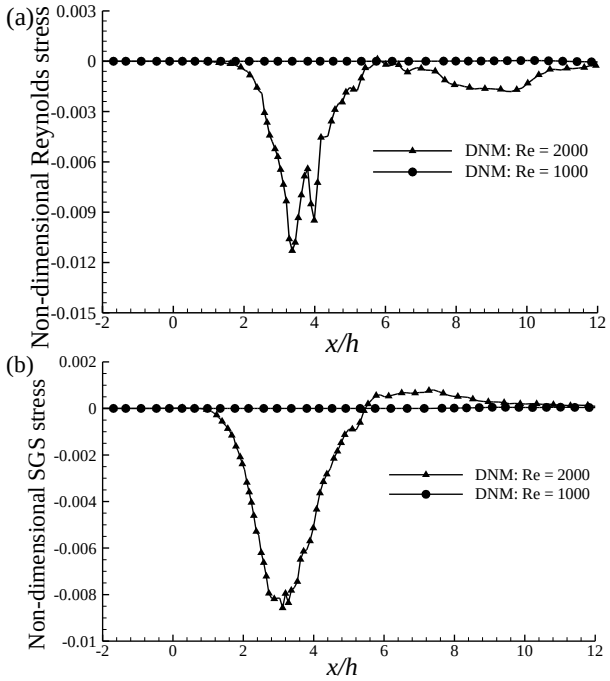

Fig 9. Non-dimensionalized shear stress (a) resolved turbulent shear stress, $-< u"v" > / \bar{U}^2$ and (b) SGS shear stress, $-< \tau_{12} > / \bar{U}^2$

Fig. 9 displays the streamwise distribution of the non-dimensionalized resolved Reynolds turbulent shear stress, $-< u"v" > / \bar{U}^2$and the SGS shear stress, $-< \tau_{12} > / \bar{U}^2$ for the two different Reynolds number tested. Both the Reynolds turbulent shear stress and SGS shear stress for *Re* = 2000 undergo a sharp drop within the recirculation region 0< *x/h* <3, due to the presence of the adverse pressure gradient, whereas for *Re* = 1000, both the shear stresses are almost zero.

5. CONCLUSIONS

The technique of LES with the dynamic non-linear model has been applied to simulate a Newtonian, incompressible and physiological pulsatile flow in a constricted channel to investigate the transition-to-turbulent flow due to the arterial stenosis. In general, the flow pattern is laminar in the upstream of the stenosis which is indicated by the very low values of the resolved Reynolds stress, SGS shear stress as well as the three model coefficients of DNM. The far downstream region shows the similar trend due to the re-laminarization followed by an increasing trend of the above mentioned quantities at the throat and immediate post-stenotic region.

Blood flow does not always behave as a Newtonian fluid in arteries. For this reason, any LES study of non-Newtonian blood flow through a stenosis based on the conventional dynamic SGS stress model of Lilly [27] may not be suitable. The constitutive relationship of the DM is based on the overly simplified linear Boussinesq assumption (Smagorinsky), and correspondingly, the SGS viscosity of the DM is a linear function of the resolved strain rate tensor. However, the molecular viscosity of a non-Newtonian blood fluid is typically a nonlinear function of the strain rate tensor. In future studies, the application of the DNM to LES of non-Newtonian blood flows can be considered, as this may successfully resolve the current conceptual inconsistency in modelling the molecular and SGS viscosities for LES based on the conventional DM.

6. REFERENCES

1. Mittal, R., Simmons, S. P. and Najjar, F., 2003, "Numerical study of pulsatile flow in a constricted channel", *J. Fluid Mech*., pp. 485: 337-378.
2. Molla, M. M., Paul, M. C. and Roditi, G., 2010, "LES of additive and non-additive pulsatile flows in a model arterial stenosis", *Comput. Meth. Biomech. Biomed. Eng*., pp. 13:105-120.
3. Lilly, D. K., 1992, "A Proposed Modification of the Germano Subgrid-Scale Closure Method", *Phys. Fluids A*, pp. 4:633-635.
4. Wang, B.-C., and Bergstrom, D. J., 2005, "A dynamic nonlinear subgrid-scale stress model", *Phys. Fluids*, pp. 17: 035109.
5. Ku, D. N., 1997, "Blood flows in arteries", *Annu. Rev. Fluid Mech*., pp. 29:399-434.
6. Bloor, M. S., 1964, "The transition to turbulence in the wake of a circular cylinder", *J. Fluid Mech*., pp. 21: 290-304.
7. Clark, C., 1976, "The fluid mechanics of aortic stenosis-I. theory and steady flow experiments", *J. Biomech*., pp. 9: 521-528.
8. Clark, C., 1976, "The fluid mechanics of aortic stenosis-II. unsteady flow experiments", *J. Biomech*., pp. 9: 567-573.
9. Cassanova, R. A. and Giddens, D. P., 1978, "Disorder distal to modeled stenoses in steady and pulsatile flow", *J. Biomech*., pp. 11: 441-453.
10. Ahmed, S. A. and Giddens, D. P., 1983, "Velocity measurements in steady flow through axisymmetric stenoses at moderate Reynolds numbers", *J. Biomech.*, pp. 16:505-516.
11. Ahmed, S. A. and Giddens, D. P., 1983, "Flow

disturbance measurements through a constricted tube at moderate Reynolds numbers", *J. Biomech.*, pp. 16:955-963.

12. Mittal, R. , Simmons, S. P. and Udaykumar, H. S., 2001, "Application of large-eddy simulation to the study of pulsatile flow in a modeled arterial stenosis", *ASME J. Biomech. Eng*., pp. 123: 325-331.
13. Molla, M. M. , Paul, M. C. and Roditi, G., 2008, "Physiological flow in a model of arterial stenosis", *J. Biomech.*, pp. 41(S1):243.
14. Kershaw, D. S., 1978, "The incomplete cholesky conjugate gradient method for the iterative solution of systems", *J. Comp. Phys.*, pp. 26: 43-65.
15. Vorst, H. A. D., 1992, "BI-CGSTAB: a first and smoothly converging variant of BI-CG for the solution of the non-symmetric linear systems", *SIAM J. Sci. Stat. Comput.*, pp. 155: 631-644.

7. NOMENCLATURE

Symbol	Meaning
Re	Reynolds number
h	Height of the channel
$\bar{U}$	Bulk velocity
P	Pressure
ρ	Fluid density
ν	Kinematic viscosity
A	Amplitude of the pulsatile oscillation
n	Number of harmonics
α	Womersely number
x,y,z	Coordinates of the Cartesian frame
t	Time
C_S, C_W, C_N	SGS stress model coefficients

8. MAILING ADDRESS

Afzal Hossain
Dept. of Mechanical and Manufacturing Engg., Univ. of Manitoba, Canada.
E-mail:Afzal_rupak@yahoo.com